

**Magnetic interface coupling between ultrathin Co and Ni<sub>x</sub>Mn<sub>100-x</sub> films on Cu(001)**M. Reinhardt, J. Seifert, M. Busch,<sup>\*</sup> and H. Winter*Institut für Physik, Humboldt Universität zu Berlin, Newtonstrasse 15, D-12489 Berlin-Adlershof, Germany*

(Received 9 December 2009; revised manuscript received 3 March 2010; published 28 April 2010)

Growth and magnetic properties of Ni<sub>x</sub>Mn<sub>100-x</sub> single and Co/Ni<sub>x</sub>Mn<sub>100-x</sub> bilayer films on Cu(001) have been investigated by grazing ion scattering, Auger electron spectroscopy, low-energy electron diffraction, and magneto-optical Kerr effect. The increase in the coercivity field strength and the decrease in the signal strength of the hysteresis loop is used as a measure of the magnetic interface coupling in the bilayers. The strength of the antiferromagnetic/ferromagnetic interface coupling rapidly increases with increasing NiMn thickness. Above a critical NiMn thickness of about 8 ML, we observe the strongest interface coupling effects in the intermediate concentration regime with a Ni content  $10 \leq x \leq 40$  at a temperature of  $T=300$  K and  $5 \leq x \leq 50$  for  $T=133$  K.

DOI: [10.1103/PhysRevB.81.134433](https://doi.org/10.1103/PhysRevB.81.134433)

PACS number(s): 75.70.-i, 75.30.Gw, 75.60.Jk, 79.20.Rf

**I. INTRODUCTION**

The functionality of modern magnetoelectronic devices is based on the interactions in thin magnetic films and, in particular, the coupling effects of a ferromagnetic (FM) to an adjacent antiferromagnetic (AFM) layer.<sup>1,2</sup> The interaction between the AFM and the FM layer increases the magnetic field, necessary to reverse the magnetization of the FM layer, and can induce an unidirectional magnetic anisotropy, which favors a defined magnetization direction. This was first observed by Meiklejohn and Bean<sup>3,4</sup> and described as a result of the interfacial exchange interaction. During the last two decades, the interest in this topic was increased due to advances in preparation and characterization of low-dimensional systems and the relevance of thin films in technology. Several model systems have been investigated theoretically and experimentally in order to understand the coupling mechanism at AFM/FM interfaces.<sup>5</sup> However, a fundamental understanding of the AFM/FM interaction is still missing. The main reason is the sensitive dependency of the coupling on the interface structure and the homogeneities of the AFM and FM layers. In this framework, structural imperfections such as interface roughness, intermixing, or even chemical interface reactions that occur during the growth process or as result of thermal treatments are important and have to be considered in realistic models.

Systems of interest are composed of the classical antiferromagnets NiO and CoO.<sup>6,7</sup> Besides these oxide based model systems, AFM metallic alloy systems have attracted considerable attention. One of the most studied AFM system is FeMn,<sup>8-13</sup> due to its experimentally convenient Néel temperature of 490 K,<sup>6</sup> and its use in exchange-biased tunnel magnetoresistance devices.<sup>14</sup> Another promising AFM model system is NiMn, which crystallizes in a face-centered tetragonal (fct) CuAu  $L1_0$  structure. The lattice constants of the  $L1_0$  phase of NiMn are  $a=b=3.74$  Å and  $c=3.52$  Å, where Ni and Mn atoms occupy alternating atomic sheets oriented perpendicular to the  $c$  axis.<sup>15,16</sup> A magnetic long-range order of equiatomic NiMn only appears in the chemically ordered  $L1_0$  phase with a Néel temperature of 1070 K.<sup>15,17</sup> The spin structure of the  $L1_0$  phase of NiMn is characterized by an antiparallel alignment of the magnetic moments of nearest-

neighbor Mn atoms, whereas these moments are oriented normal to the  $c$  axis of the fct lattice.<sup>17-20</sup>

In the last decade, several studies on NiMn were performed in the regime of thin and ultrathin films.<sup>21-31</sup> In an x-ray magnetic circular dichroism study of  $c(2 \times 2)$  NiMn/Ni(001) an FM instead of an AFM order was observed and attributed to the lattice distortion.<sup>23,24</sup> An FM order has also been observed for Ni<sub>x</sub>Mn<sub>100-x</sub> films on Cu(001) with a Ni content  $x \geq 80$ .<sup>28</sup> These films were found to exhibit a Ni-type spin-reorientation transition from in plane to out of plane upon increasing the film thickness. A noncollinear spin density was observed by spin-polarized scanning tunneling microscopy on equiatomic NiMn films grown layer by layer on Cu(001).<sup>31</sup> This finding deviates significantly from the expected collinear alignment and was interpreted by a surface reconstruction.

Tieg *et al.*<sup>30</sup> have shown using medium-energy electron diffraction (MEED), that Co grows layer by layer and observed a  $p(1 \times 1)$  structure on an equiatomic  $c(2 \times 2)$  NiMn film grown on Cu(001) at room temperature. The  $p(1 \times 1)$  low-energy electron-diffraction (LEED) patterns of nonequiatomic NiMn films on Cu(001) were interpreted by the absence of chemical order in these films, which is in agreement with the bulk-phase properties. Using Co/Cu(001) as a substrate for equiatomic NiMn films, they observed a nonlayer-by-layer growth of the alloy films and diffuse LEED patterns with weak  $c(2 \times 2)$  spots only. Based on magneto-optical Kerr effect (MOKE) measurements, Tieg *et al.* concluded from the coercivity enhancement the presence of an antiferromagnetic order in Ni<sub>x</sub>Mn<sub>100-x</sub> films with a Ni content  $x$  close to the equiatomic composition and thickness above 8 ML at room temperature.

In this paper, we present the results of investigations on the structural and magnetic properties of molecular-beam epitaxy (MBE)-grown Ni<sub>x</sub>Mn<sub>100-x</sub> single and Co/Ni<sub>x</sub>Mn<sub>100-x</sub> bilayers on a Cu(001) substrate over the full concentration range. The Ni<sub>x</sub>Mn<sub>100-x</sub> layer thickness was systematically varied in the ultrathin film limit with total thickness below 25 ML. The measurements on the magnetization of the whole Co film as well as the topmost Co surface layer were performed in a temperature range from  $T=300$  K down to about 130 K.

## II. EXPERIMENT

The experiments were performed in an ultrahigh-vacuum chamber at a base pressure in the  $10^{-11}$  mbar range, attached via two differential pumping stages to the beamline of a small electrostatic ion accelerator. The Cu(001) single crystal was prepared by cycles of grazing sputtering with 25 keV Ar<sup>+</sup> ions and subsequent annealing at 770 K for about 20 min. Mn, Ni, and Co (purity: Mn: 99.99%, Ni, Co: 99.995%) were deposited by molecular-beam epitaxy at rates of 0.5–1 ML/min with the substrate held at room temperature. The Ni<sub>x</sub>Mn<sub>100-x</sub> films were produced by simultaneous deposition of Ni and Mn from two different electron-beam evaporators EFM3 (Omicron). The alloy compositions were achieved by adjusting the individual deposition rates and inspected by Auger electron spectroscopy using an electron gun LEG32 (VG scienta) and a CLAM spectrometer (VG scienta). The crystalline structure of substrate and film were investigated by LEED using a SPA-LEED (spot profile analysis-low energy electron diffraction) instrument (Omicron).

The experiments with atomic projectiles were performed with well collimated beams of H and He atoms or ions with energies of some 10 keV. The beams were directed on the crystal surface at polar angles of incidence  $\Phi_{\text{in}} \approx 1.6^\circ$  with respect to the surface plane. In order to study film growth, the intensity of specularly reflected 25 keV He atoms was recorded with a channeltron as a function of the deposition time.

In ion beam triangulation (IBT) (Refs. 32 and 33) studies, the ion-induced emission of electrons was monitored as a function of the azimuthal angle of incidence  $\Theta$  for grazing scattering of 29 keV H atoms. The emitted electrons were detected by a surface barrier detector (SBD, Canberra) (Ref. 34) positioned at a distance of about 0.1 m above the target surface. The SBD was biased to a high voltage of about 20 kV, where the pulse height is proportional to the number of emitted electrons per scattering event. This allows one to study electron number spectra.<sup>35</sup> The discriminator level of the SBD was set to a pulse height interval which is equivalent to electron numbers from about two to four electrons. This signal was normalized to the overall detected electrons. Since the penetration of projectiles into the bulk for scattering along low-indexed axial channels results in an enhancement of the electron yield, the arrangement of atomic strings (i.e., low-index crystalline directions) in the surface is identified by the reduction in the signal for events, related to the emission of lower electron numbers for scattering along random (high-index) directions. For low electron numbers, the information depth is restricted to the topmost surface layer. A more detailed discussion on the IBT method is given elsewhere.<sup>36,37</sup>

For the scattering experiments on electron capture (EC) into excited levels of He atoms, the emitted polarized fluorescence light of the  $1s3p\ ^3P \rightarrow 1s2s\ ^3S$  transition at  $\lambda = 388.9$  nm was detected through a quartz window by means of a quarter-wave retarder plate, a narrow bandwidth interference filter, a linear polarizer, and a cooled photomultiplier. The concepts and analysis of experiments on polarized light emission after electron capture are described in detail in Refs. 38–40. In brief, the spin polarization  $P_s$  of captured

electrons can be deduced from the circular polarization of the fluorescence light described by the Stokes parameter  $S/I = [I(\sigma^-) - I(\sigma^+)] / [I(\sigma^-) + I(\sigma^+)]$ , where  $I(\sigma^-)$  and  $I(\sigma^+)$  are the intensities of light with negative and positive helicities,  $\sigma^-$  and  $\sigma^+$ , respectively.<sup>41</sup> The spin polarization  $P_s$  is obtained from measurements of the Stokes parameter  $S/I(\uparrow)$  and  $S/I(\downarrow)$  with reversed settings of the magnetization.  $P_s$  and  $\Delta S/I = S/I(\uparrow) - S/I(\downarrow)$  are related to the long-range magnetic order of the topmost atomic layer of the surface (probing depth  $\lambda_{\text{EC}} \rightarrow 0$  ML),<sup>42–45</sup> although a quantitative relation has not been established so far.

The behavior of the magnetization of the total film was observed by making use of MOKE in the longitudinal geometry. In order to record hysteresis loops, the change in the intensity of light from an electronically stabilized laser diode ( $\lambda = 635$  nm) that passes through an analyzing polarizer (set to an angle close to extinction) is monitored as the applied magnetic field is swept.<sup>46</sup> The peak-to-peak intensity  $\Delta I_{\text{MOKE}}$ , which is the difference in MOKE intensities, at positive and negative saturation magnetizations, is related to the amount of Kerr rotation and, in the case of thin films, to the total magnetic moment.<sup>46,47</sup> The normalized MOKE signal  $\hat{\Delta I}_{\text{MOKE}}$  can be expressed in percentage by the ratio between  $\Delta I_{\text{MOKE}}$  and the MOKE intensity  $I_{\text{MOKE}}$  at negative or positive saturation. The hysteresis loops were recorded for magnetic fields ranging from  $-200$  to  $+200$  Oe (1 Oe = 79.6 A/m), which were generated by external Helmholtz coils. Sample temperatures down to about 130 K were achieved by cooling the sample holder (VG scienta) with liquid nitrogen.

## III. RESULTS AND DISCUSSION

### A. Growth, chemical composition, and crystalline structure

In Fig. 1, we display the normalized intensity of specularly reflected 25 keV He atoms, recorded during the simultaneous deposition of Ni and Mn for different individual deposition rates at room temperature. The observed intensity oscillations reflect the periodic changes in the film morphology,<sup>48</sup> where an intensity maximum corresponds to a film with less roughness, i.e., a completed layer. In analogy to the system Fe<sub>x</sub>Mn<sub>100-x</sub>/Cu(001) (Refs. 10, 12, and 13) three regimes of growth behavior can be classified: a Mn-rich, an intermediate, and a Ni-rich regime. For both systems the intensity oscillations are strongly damped during the growth of Mn-rich films. For pure Mn growth, only the first intensity maximum corresponding to the first monolayer of a Cu-Mn alloy<sup>49</sup> can be identified. The overall drop in intensity corresponds to three-dimensional (3D) island growth and an increasing surface roughness due to the lattice mismatch.

The number of intensity oscillations and their amplitudes increase continuously with increasing Ni content. For Ni<sub>21</sub>Mn<sub>79</sub> weak oscillations up to a coverage of 10 ML can be identified. For a Ni content of 36%, oscillations were maintained up to coverages of more than 10 ML. Tieg *et al.*<sup>30</sup> observed MEED intensity oscillations for a Ni content above 40% only. In the range close to equiatomic concentrations of Ni and Mn, the amplitudes of the oscillations were only

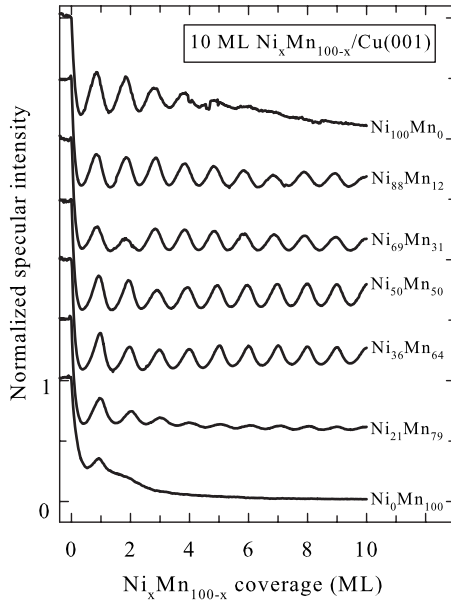


FIG. 1. Normalized intensity of specularly reflected 25 keV He atoms ( $\Phi_{\text{in}}=1.6^\circ$ ) recorded during simultaneous deposition of Ni and Mn on Cu(001) at room temperature for different individual deposition rates. Curves are shifted equidistantly with respect to data for  $\text{Ni}_0\text{Mn}_{100}$  (bottom).

slightly damped even for high coverages, indicating an almost perfect layer-by-layer growth. For pure Ni growth, the amplitudes of the oscillations decrease for coverages above 4 ML due to the continuous transition from layer-by-layer to multilayer growth and subsequent 3D island growth.<sup>28,50,51</sup>

The growth of the pure films (bottom and top in Fig. 1) provides the correct positioning and calibration of the Ni and Mn electron-beam evaporators. Different alloy compositions are obtained by adjusting the individual deposition rates. The final quantitative determination of the chemical composition (given at the right side in Figs. 1 and 2) follows from Auger electron spectroscopy after growth of the films. Corresponding numerically differentiated spectra  $dI/dE$  for the excitation by 4 keV primary electrons (polar angle of incidence  $\Phi_{\text{in}}=30^\circ$  with respect to the surface plane) are shown in Fig. 2. The LMM Auger transitions of the elements Mn, Ni, and Cu extend over an electron energy range from 500 up to 920 eV, whereas the Ni and Cu Auger signals are partly superimposed. The element-specific energies of the Auger transitions are given at the bottom (for Mn and Cu) and at the top (for Ni) of Fig. 2. The relative heights of the Ni and Mn Auger signals change with alloy composition and, therefore, we obtained the relative amounts of both elements from the peak-to-peak heights  $\Delta I$  of the pronounced Mn LMM signal at 589 eV and the Ni LMM signal at 716 eV, which is slightly separated from the Cu Auger signals. Element specific Auger electron cross sections are taken into account by the relative Auger sensitivities:  $S_{\text{Mn}}(589 \text{ eV})=7.45$  and  $S_{\text{Ni}}(716 \text{ eV})=2.05$ .<sup>52</sup> The contents  $x_{\text{Mn}}$  and  $x_{\text{Ni}}=x$  of Mn and Ni, respectively, are given by:  $x_{\text{Mn}} = \frac{\Delta I_{\text{Mn}}/S_{\text{Mn}}}{\Delta I_{\text{Mn}}/S_{\text{Mn}} + \Delta I_{\text{Ni}}/S_{\text{Ni}}}$  and  $x_{\text{Ni}} = \frac{\Delta I_{\text{Ni}}/S_{\text{Ni}}}{\Delta I_{\text{Mn}}/S_{\text{Mn}} + \Delta I_{\text{Ni}}/S_{\text{Ni}}}$ . The alloy compositions were determined with an accuracy of about  $\pm 5\%$  and checked by comparison of the time period of the growth oscillations for the alloy films with the pure Ni film for constant Ni deposition rate.

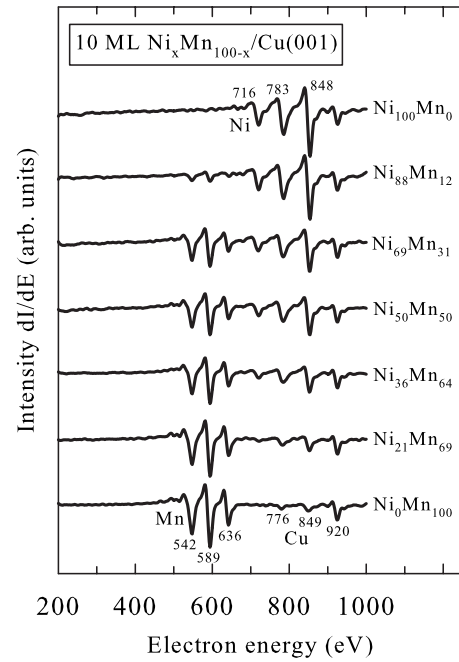


FIG. 2. Auger spectra of 10 ML  $\text{Ni}_x\text{Mn}_{100-x}$  films with different alloy compositions (primary electron energy: 4 keV).

The probing depth of the Mn and Ni LMM-Auger electrons amounts to approximately 5–6 ML,<sup>53,54</sup> i.e., averaging over a substantial part of the total film. Due to the higher probing depth of about 8 ML (Refs. 53 and 54) of the Cu LMM-Auger electrons with an energy of 920 eV, the corresponding Cu Auger signal is still present for a  $\text{Ni}_x\text{Mn}_{100-x}$  coverage of 10 ML.

The crystalline structure of the  $\text{Ni}_x\text{Mn}_{100-x}$  alloy films was investigated using LEED and IBT. In Fig. 3, we show LEED patterns for clean Cu(001), 10 ML  $\text{Ni}_{50}\text{Mn}_{50}$  and 10 ML  $\text{Ni}_{35}\text{Mn}_{65}$  on Cu(001), which are recorded at an electron energy of 125 eV. The primitive square lattice of Cu(001) can be identified in the  $p(1 \times 1)$  pattern in the left panel of Fig. 3. The middle panel shows the  $c(2 \times 2)$  pattern of the  $\text{Ni}_{50}\text{Mn}_{50}$  film. This result is in accord with the observation of a  $c(2 \times 2)$  pattern in an  $I(E)$ -LEED study, which was interpreted as a result of the chemical order in a  $\text{Ni}_{50}\text{Mn}_{50}$  film on Cu(001) in combination with a reconstruction of the topmost surface layer.<sup>30</sup> Such an equiatomic NiMn film shows a CuAu-I face-centered tetragonal structure, where Ni and Mn atoms occupy alternating atomic sheets oriented perpendicular to the Cu(001) surface.<sup>15,31</sup> The  $c(2 \times 2)$  superstructure of

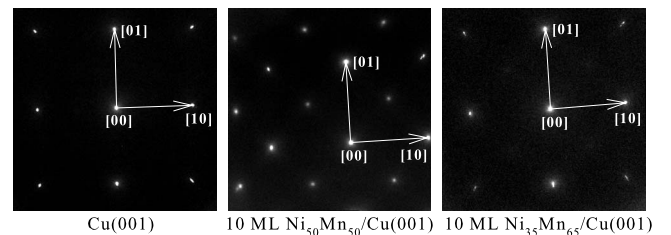


FIG. 3. LEED patterns for clean Cu(001) (left), 10 ML  $\text{Ni}_{50}\text{Mn}_{50}$  (middle), and 10 ML  $\text{Ni}_{35}\text{Mn}_{65}$  (right) on Cu(001) for electron energy of 125 eV.

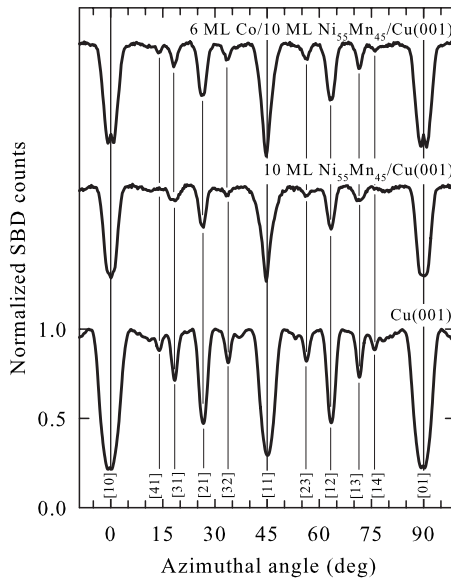


FIG. 4. Normalized surface barrier detector (SBD) counts versus azimuthal angle of incidence for grazing scattering of 29 keV H atoms ( $\Phi_{\text{in}}=1.6^\circ$ ) from clean Cu(001) (bottom), 10 ML  $\text{Ni}_{55}\text{Mn}_{45}$  (middle), and 6 ML Co/10 ML  $\text{Ni}_{55}\text{Mn}_{45}$  (top) on Cu(001). IBT curves are shifted vertically.

equiatomic NiMn films can be explained by a bulklike crystal structure throughout the whole film and is stabilized by the small lattice mismatch of the  $L1_0$  bulk phase with respect to the Cu(001) substrate.<sup>30</sup> However, for Ni- and Mn-rich alloy films on Cu(001) a  $p(1 \times 1)$  pattern is observed for the chemically disordered and an enhanced tetragonal distorted structure due to the lattice mismatch with the substrate<sup>28</sup> (cf. right panel of Fig. 3).

We performed also IBT measurements on the atomic structure of the topmost surface layer in real space by making use of surface channeling phenomena for grazing atom scattering. The results are displayed in Fig. 4. For the clean fcc(001) surface of Cu, the IBT curve shows pronounced minima at low-index directions  $[uv]$  in the primitive square surface lattice. Such pronounced minima at the directions  $[10]$ ,  $[21]$ ,  $[11]$ ,  $[12]$ , and  $[01]$  were also observed for 10 ML  $\text{Ni}_{55}\text{Mn}_{45}$  on Cu(001). Therefore, we conclude that the surface of the alloy films retains the initial structure of Cu(001). The decrease in the minima results from a slight increase in the surface roughness. For a coverage of 6 ML Co on 10 ML  $\text{Ni}_{55}\text{Mn}_{45}$ /Cu(001) the initial structure is preserved (cf. Fig. 4).

The growth of Co on top of 10 ML  $\text{Ni}_x\text{Mn}_{100-x}$  on Cu(001) also proceeds layer by layer in the intermediate concentration regime with a Ni content  $30\% \leq x_{\text{Ni}} \leq 80\%$  (cf. Fig. 5). This finding is in accord with the results in Ref. 30, where MEED oscillations were observed for the growth of 4 ML Co on 12 ML  $\text{Ni}_{50}\text{Mn}_{50}$ /Cu(001) at  $T=300$  K. A similar behavior was found for the system 6 ML Co/15 ML  $\text{Fe}_x\text{Mn}_{100-x}$ /Cu(001) in the intermediate concentration regime.<sup>13</sup>

For the investigation of the magnetic properties as function of NiMn thickness, we increased the coverage of NiMn layer by layer on top of a 6 ML Co film on Cu(001). In

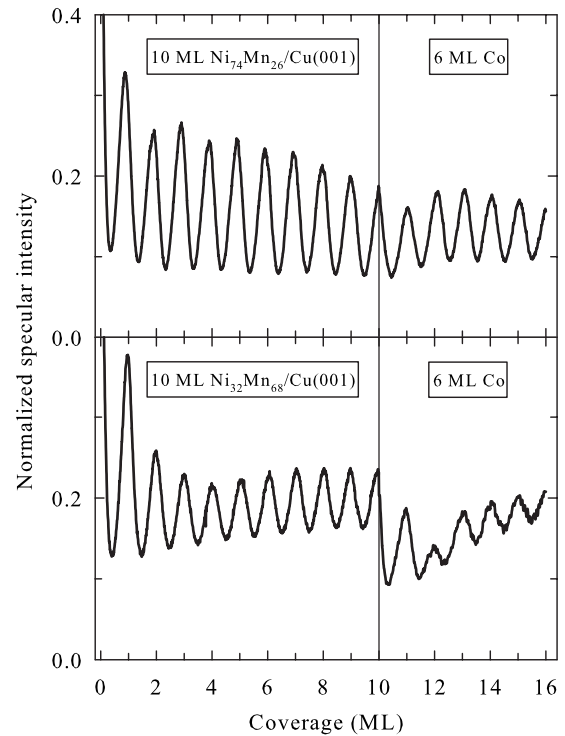


FIG. 5. Normalized intensity of reflected 25 keV He atoms ( $\Phi_{\text{in}}=1.6^\circ$ ) for deposition of 6 ML Co on 10 ML  $\text{Ni}_{74}\text{Mn}_{26}$  (top) and on 10 ML  $\text{Ni}_{32}\text{Mn}_{68}$  (bottom) on Cu(001) at room temperature.

Fig. 6, we display the normalized intensity of reflected 25 keV He atoms for the deposition of 20 ML  $\text{Ni}_{35}\text{Mn}_{65}$  and 20 ML  $\text{Ni}_{45}\text{Mn}_{55}$  at room temperature. We found pronounced intensity oscillations during the layer-by-layer growth of  $\text{Ni}_{35}\text{Mn}_{65}$ , whereas the intensity oscillations are damped for  $\text{Ni}_{45}\text{Mn}_{55}$ . However, for the 3D growth of 20 ML  $\text{Ni}_{50}\text{Mn}_{50}$  on top of a 5 ML Co film on Cu(001) only a decay of MEED intensities without oscillations were reported in Ref. 30.

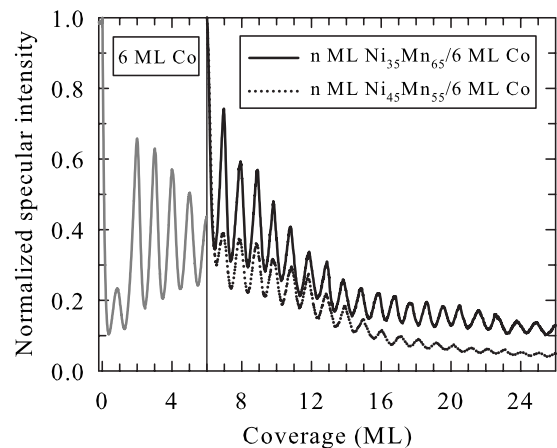


FIG. 6. Normalized intensity of reflected 25 keV He atoms ( $\Phi_{\text{in}}=1.6^\circ$ ) for deposition of 20 ML  $\text{Ni}_{35}\text{Mn}_{65}$  (solid black curve) and 20 ML  $\text{Ni}_{45}\text{Mn}_{55}$  (dotted black curve) on 6 ML Co (gray solid curve) on Cu(001) at room temperature. Solid and dotted black curve are normalized.

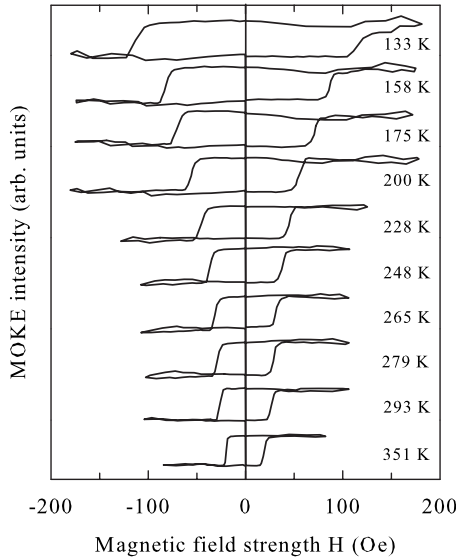


FIG. 7. MOKE hysteresis loops recorded with decreasing temperature from  $T=351$  to 133 K for a 6 ML Co/7 ML  $\text{Ni}_{50}\text{Mn}_{50}$  bilayer film.

**B. Thickness, chemical composition, and temperature-dependent magnetic properties**

The magnetic order of the epitaxial NiMn films was studied by MOKE and EC measurements performed on NiMn/Co and Co/NiMn bilayers on Cu(001). The MOKE hysteresis loops were measured in the longitudinal geometry with an external magnetic field  $H$  applied along the  $\langle 110 \rangle = [10]$  direction, the magnetic easy axis of an epitaxial Co film on Cu(001) and for Co films on top of paramagnetic FeMn.<sup>55-58</sup> For AFM/FM interfacial exchange coupling, the bilayer system ought to show the characteristic coercivity enhancement. This is an indirect evidence for the AFM order in the NiMn layer. In Fig. 7, we display MOKE hysteresis loops recorded with decreasing temperature from  $T=351$  to 133 K for a 6 ML Co/7 ML  $\text{Ni}_{50}\text{Mn}_{50}$  bilayer film. The coercivity  $H_C$  significantly increases with decreasing temperature  $T$  while the hysteresis loops retain their close to rectangular shape.

The temperature-dependent coercivity enhancement was also investigated for Co/ $\text{Ni}_{50}\text{Mn}_{50}$  bilayers for a different  $\text{Ni}_{50}\text{Mn}_{50}$  thickness. The results are shown in Fig. 8. With increasing  $\text{Ni}_{50}\text{Mn}_{50}$  thickness, the onset of the coercivity enhancement shifts to higher temperatures for a constant Co coverage of 6 ML. For a  $\text{Ni}_{50}\text{Mn}_{50}$  thickness above 7 ML, the coercivity is increased for  $T=300$  K. The slight shift of the data for 7 ML NiMn in Fig. 8 results from deviations of the Ni and Mn concentrations from the perfect equiatomic ratio. For comparison, we also plot in Fig. 8 the coercivity  $H_C$  measured in a recent study on 6 ML Co/6 ML  $\text{Fe}_{50}\text{Mn}_{50}/\text{Cu}(001)$  for decreasing temperature. At  $T=300$  K, the coercivity  $H_C$  of both bilayer systems is nearly unchanged compared to a single Co film. However, for  $T=200$  K, the coercivity  $H_C \approx 80$  Oe of 6 ML Co/6 ML  $\text{Fe}_{50}\text{Mn}_{50}/\text{Cu}(001)$  is larger by a factor of 4 with respect to  $H_C$  measured on 6 ML Co/6 ML  $\text{Ni}_{50}\text{Mn}_{50}/\text{Cu}(001)$  caused by a higher AFM anisotropy in the FeMn layer.

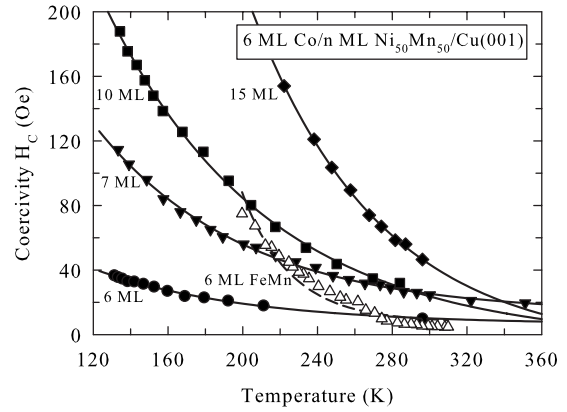


FIG. 8. Coercivity  $H_C$  as function of temperature for 6 ML Co/ $n$  ML  $\text{Ni}_{50}\text{Mn}_{50}$  bilayers with different NiMn thickness (full symbols) and for a 6 ML Co/6 ML  $\text{Fe}_{50}\text{Mn}_{50}$  bilayer (open triangles). Curves are guide to eye.

The onset of the AFM order in the NiMn film with a thickness of about 7 ML at room temperature was also observed for the reversed deposition order. The results of the MOKE measurements on  $\text{Ni}_{35}\text{Mn}_{65}$  and  $\text{Ni}_{45}\text{Mn}_{55}$  films grown layer by layer on 6 ML Co at room temperature are shown in Fig. 9. For both bilayer films, a distinct broadening of the hysteresis loops was observed above 7–8 ML, which further increases with the NiMn coverage. This finding is in accord with the results shown in Ref. 30 for a  $\text{Ni}_{50}\text{Mn}_{50}$  film on 6 ML Co. However, the slope of  $H_C$  is more pronounced for the  $\text{Ni}_{35}\text{Mn}_{65}$  film. For the reversed concentration ratio, i.e., for a  $\text{Ni}_{65}\text{Mn}_{35}$  film on 6 ML Co/Cu(001), the magnetization reversal of the Co film of the bilayer system was unchanged in comparison to a single 6 ML Co layer on Cu(001) with  $H_C=5$  Oe at  $T=300$  K as reported in Ref. 30.

The enhancement of  $H_C$  in exchange-coupled AFM/FM bilayer systems can be attributed to irreversible changes in the AFM spin structure during magnetization reversal of the FM.<sup>6</sup> When the FM magnetization changes its direction, the coupled FM spins “drag” the AFM spins irreversibly. Thus, an additional AFM-induced anisotropy energy has to be overcome and the coercivity  $H_C$  is enhanced. The irrevers-

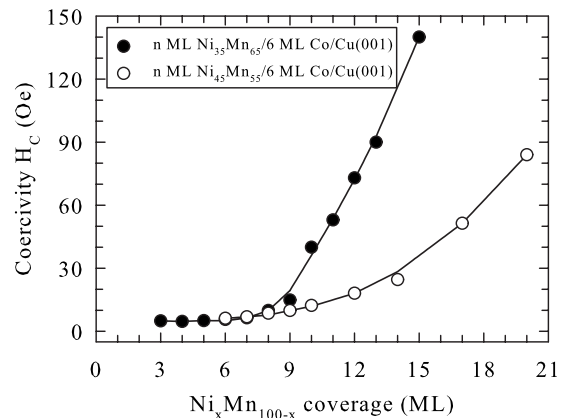


FIG. 9. Coercivity  $H_C$  for  $n$  ML  $\text{Ni}_{35}\text{Mn}_{65}/6$  ML Co (full circles) and  $n$  ML  $\text{Ni}_{45}\text{Mn}_{55}/6$  ML Co (open circles) bilayers with different NiMn thickness at  $T=300$  K. Curves are guide to eye.

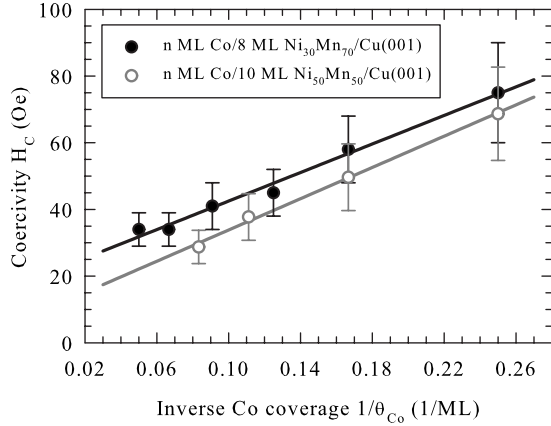


FIG. 10. Coercivity  $H_C$  for  $n$  ML Co/8 ML  $\text{Ni}_{30}\text{Mn}_{70}$  (full black circles) and  $n$  ML Co/10 ML  $\text{Ni}_{50}\text{Mn}_{50}$  (open gray circles) bilayers as function of inverse Co coverage  $1/\theta_{\text{Co}}$  at  $T=300$  K. Black and gray line: best linear fits to data (for details, see text).

ible processes in the AFM film dominate the hysteresis loop behavior for a small AFM anisotropy energy. This holds for a thin AFM film or if the temperature is close to the AFM ordering temperature.<sup>6</sup> The increase in the coercivity  $H_C$  with decreasing temperature originates from an increase in AFM anisotropy. Thus, higher external fields are required to drag AFM spins during magnetization reversal at low temperatures. For a sufficiently high AFM anisotropy, the exchange coupling between an AFM and a FM layer manifests itself in a shift  $H_{\text{ex}}$  of the hysteresis loop from zero field. This “exchange bias”<sup>3-7</sup> occurs if the system is cooled below the Néel temperature in an external magnetic field or for an external magnetic field applied during film deposition. In a simple model, the interfacial interaction between the FM spins and the aligned AFM spins at the interface prevent the magnetization reversal of the ferromagnet. However, in our studies on Co/NiMn/Cu(001) no significant shift ( $H_{\text{ex}} \leq 5$  Oe) of MOKE hysteresis loops was observed for various film thicknesses and compositions.

For exchange-coupled AFM/FM bilayer systems, the interfacial interaction leads to a decrease in the coercivity  $H_C$  for increasing FM thickness  $\theta_{\text{FM}}$ . In the model of Stiles and McMichael,<sup>59</sup> energy losses due to irreversible processes in the AFM during magnetization reversal are present at temperatures  $T > 0$  K and cause a coercivity dependence on the FM thickness proportional to  $\theta_{\text{FM}}^{-1}$ . A second contribution to  $H_C$  arises from an inhomogeneous magnetization reversal of the FM, leading to a  $\theta_{\text{FM}}^{-2}$  dependence of  $H_C$ . Although the model describes polycrystalline bilayers, it may be also applicable to crystalline epitaxial thin films.<sup>60</sup> In Fig. 10 we show  $H_C$  for  $n$  ML Co/8 ML  $\text{Ni}_{30}\text{Mn}_{70}$  and  $n$  ML Co/10 ML  $\text{Ni}_{50}\text{Mn}_{50}$  bilayers as function of the inverse Co coverage  $1/\theta_{\text{Co}}$  measured at  $T=300$  K. The data were fitted with the linear function  $H_C(\theta_{\text{Co}}) = H_C(\infty) + A/\theta_{\text{Co}}$ , where  $H_C(\infty)$  and  $A$  denote the coercivity for infinite Co coverage and a fit parameter, respectively. As observed for NiMn/Co bilayers (cf. Fig. 9)  $H_C$  is higher for a Mn-rich alloy film, even for a lower thickness of 8 ML  $\text{Ni}_{30}\text{Mn}_{70}$  compared to 10 ML of the equiatomic NiMn film. However, the linear dependence of the coercivity  $H_C$  on the inverse Co coverage  $1/\theta_{\text{Co}}$  for both

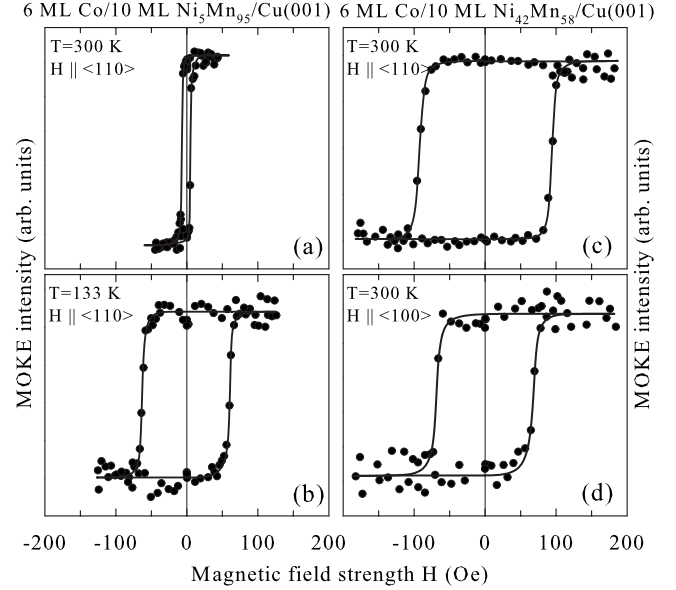


FIG. 11. MOKE hysteresis loops for 6 ML Co/10 ML  $\text{Ni}_5\text{Mn}_{95}$  (panels a and b) and 6 ML Co/10 ML  $\text{Ni}_{42}\text{Mn}_{58}$  (panels c and d) bilayer on Cu(001) with external magnetic field  $H$  applied along directions  $\langle 110 \rangle = [10]$  (panels a-c) and  $\langle 100 \rangle = [11]$  (panel d) at  $T=300$  K (panels a, c, and d) and  $T=133$  K (panel b).

bilayer systems is in accord with the finding in Ref. 30 for a Co film on an equiatomic 12.2 ML NiMn film. This is in line with a small AFM anisotropy and irreversible changes in the AFM spin structure dominate the magnetization reversal.

A considerably enhanced  $H_C$  is also observed for low Ni contents at low temperatures. In Fig. 11(a), we show a MOKE hysteresis loop measured for 6 ML Co/10 ML  $\text{Ni}_5\text{Mn}_{95}$  bilayers at  $T=300$  K, which is in accord with the hysteresis loop for 6 ML Co/Cu(001) (not shown). A hysteresis loop measured for 6 ML Co/10 ML  $\text{Ni}_5\text{Mn}_{95}$  at  $T=133$  K is displayed in Fig. 11(b). The coercivities are different by a factor of about 12 and indicate an AFM order in  $\text{Ni}_x\text{Mn}_{100-x}$  films with low Ni content at low temperatures.

Aside from the enhancement of the coercivity, the AFM/FM coupling can change the orientation of the easy axis of the FM film. This was observed, for example, for Co/ $\text{Fe}_{50}\text{Mn}_{50}$  bilayers on Cu(001) for a Co thickness below 15 ML and an FeMn thickness above 10 ML.<sup>9,10</sup> The change in the magnetic easy axis from  $\langle 110 \rangle$  to  $\langle 100 \rangle$  in the Co film was related to the AFM order and uncompensated spin moments at step edges of the FeMn film. For a Co thickness above 15 ML, the Co magnetization on top of the equiatomic FeMn layer was found to be along  $\langle 110 \rangle$  directions due to the increasing total anisotropy energy in the Co film with respect to the anisotropy energy of the FeMn film. However, for Co/NiMn bilayers, we found a higher coercivity  $H_C$  for the magnetization in an external magnetic field  $H$  applied along directions  $\langle 110 \rangle$  [cf. Fig. 11(c)] compared to the magnetization along  $\langle 100 \rangle$  [cf. Fig. 11(d)]. This behavior was found over the whole Ni and Mn concentration range for different Co thickness at  $T=133$  and 300 K. Thus, an antiferromagnetic NiMn layer exchange coupling to a ferromagnetic Co layer does not change the easy axis of the Co layer.

In order to study the observed onset of AFM order for lower Ni contents  $x < 50$  (cf. Figs. 7 and 8) in more detail,

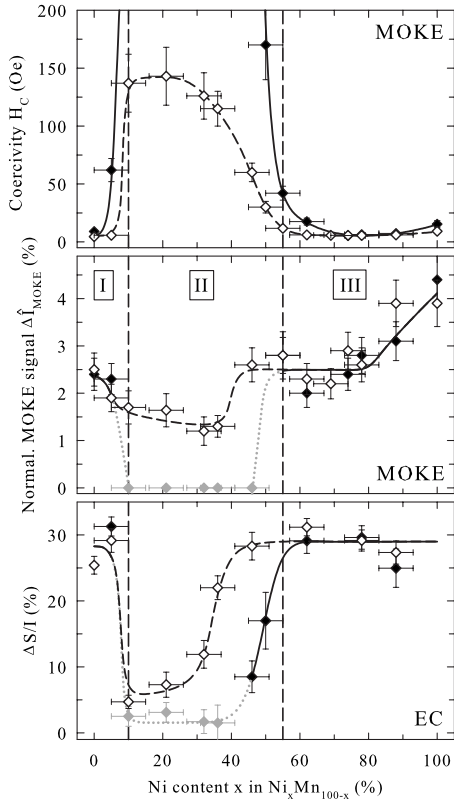


FIG. 12. Coercivity  $H_C$  (upper panel), normalized MOKE signal  $\Delta\hat{I}_{\text{MOKE}}$  (middle panel), and  $\Delta S/I$  obtained from hysteresis loops recorded by electron capture (EC, lower panel) for 6 ML Co/10 ML  $\text{Ni}_x\text{Mn}_{100-x}$  bilayers as function of Ni content  $x$  at  $T=300$  K (open diamonds) and 133 K (full diamonds). Curves are guides for eyes. Gray full diamonds: maximum accessible field of  $H = \pm 200$  Oe is not sufficient for reversal of magnetization and complete MOKE hysteresis loops cannot be recorded. For details see text.

we performed MOKE and EC measurements for 6 ML Co/10 ML  $\text{Ni}_x\text{Mn}_{100-x}$  bilayers on Cu(001) over the complete concentration range. The results are shown in Fig. 12. On the Mn-rich side (region I), the coercivity  $H_C$  increases rapidly (cf. upper panel of Fig. 12), while the normalized MOKE signal  $\Delta\hat{I}_{\text{MOKE}}$ , (cf. middle panel of Fig. 12), decreases with increasing Ni content. For a Ni content of  $x=10$ , the normalized MOKE signal  $\Delta\hat{I}_{\text{MOKE}}$  is about 1.7% at room temperature, but is not determinable for a temperature of  $T=133$  K, since it is not possible to overcome the AFM-induced enhanced magnetic anisotropy energy of the ferromagnet. Then a complete hysteresis loop cannot be recorded because the maximum accessible field of  $H = \pm 200$  Oe is not sufficient for a reversal of magnetization. This is valid at  $T=133$  K for a Ni content of  $10 \leq x \leq 45$  (region II) and indicates the strong pinning of the ferromagnetic Co film on the antiferromagnetic NiMn film due to the interface coupling. For this Ni concentration range, the values of the normalized MOKE signal  $\Delta\hat{I}_{\text{MOKE}}$  were set to 0 and plotted as gray full diamonds in the middle panel of Fig. 12. However, at room temperature the normalized MOKE signal  $\Delta\hat{I}_{\text{MOKE}} \approx 2.5\%$  measured for 6 ML Co/10 ML  $\text{Ni}_{45}\text{Mn}_{55}$  is equal to the value measured on 6 ML Co/10 ML Mn while the coercivity is still

enhanced by a factor of 10 with respect to the Co/Mn bilayer. For a Ni content above  $x=60$  (Ni-rich film, region III),  $H_C$  is not enhanced with respect to 6 ML Co/Cu(001) for temperatures  $T=133$  and 300 K. The MOKE signal is similar as for 6 ML Co/Cu(001), so we conclude that NiMn that is in a paramagnetic state. For a Ni content above  $x=80$ , the normalized MOKE signal  $\Delta\hat{I}_{\text{MOKE}}$  increases up to about 5%. This indicates a transition from the paramagnetic to the ferromagnetic order in the Ni-rich film. The present classification of the dependence of  $H_C$  and  $\Delta\hat{I}_{\text{MOKE}}$  on the alloy composition in three regions is similar as for the system Co/FeMn/Cu(001) in the regime of thin films.<sup>13</sup>

For a Ni content of  $10 \leq x \leq 40$  (region II),  $H_C$  hardly changes in this concentration range despite a significant modification of interface morphology due to different growth of NiMn on Cu(001) ranging from 3D islands for  $x=10$  to almost perfect layer-by-layer growth for  $x=40$ . The density of step edges at the interface is closely related to the strength of interface coupling.<sup>6,7</sup> As the similar FM/AFM system Co/FeMn shows a pronounced dependence on the step density<sup>9</sup> and the antiferromagnetic NiMn surface was found to have an in-plane compensated spin density,<sup>31</sup> the interplay of exchange coupling and AFM anisotropy has to be investigated for half-filled monolayers. For a Ni content of  $10 \leq x \leq 40$  at room temperature and  $5 \leq x \leq 50$  at low temperature ( $T=133$  K),  $H_C$  is highest and, therefore, the AFM anisotropy is strongest, when assuming irreversible changes in the AFM as origin for the enhancement of  $H_C$ . The presence of exchange anisotropy effects despite the chemical disorder as concluded from the absence of  $c(2 \times 2)$  superstructure LEED spots for a Ni content of  $x=30$  (cf. right panel of Fig. 3) disproves the direct correlation between chemical and magnetic order in the alloy film as assumed in Ref. 30. For bulk NiMn the antiferromagnetic  $L1_0$  phase is established for a Ni content of  $45 \leq x \leq 55$  and partial in the disordered fcc Mn phase with  $x < 45$ .<sup>15,17,61</sup> The presence of antiferromagnetic order in the thin film limit may be supported by the interlayer distance. This is only slightly enhanced for a Ni content of  $x \leq 50$  compared to the bulk NiMn  $L1_0$  phase, whereas it decreases considerably for  $x > 50$ .<sup>30</sup>

The MOKE measurements provide depth information on the magnetization averaged over the whole Co film including both interfaces between the NiMn and Co film as well as the topmost Co surface layer. However, experimental studies on thin ferromagnetic films with a thickness of several monolayers to about 100 Å, confirm significant differences in the orientation of the interface and bulk magnetization during reversal in an external magnetic field. These findings have either been attributed to weakened exchange interactions at the interface<sup>43,62</sup> or to interface-induced anisotropies.<sup>63</sup> If a ferromagnetic layer is exchange coupled to an antiferromagnetic layer, differences in the direction of the surface, interface, and bulk magnetization can occur due to the AFM-induced anisotropy at the AFM/FM interface and the formation of partial domain walls within the ferromagnetic film parallel to the surface. Such a partial domain wall can develop in the ferromagnetic film during magnetization reversal with spin rotations parallel to the interface depending on the thickness of the ferromagnetic film.<sup>5,64</sup> In ultrathin

films, such noncollinearities between surface and bulk magnetizations are expected to be small but detectable via comparison of MOKE with a method of information depth restricted to the topmost surface layer ( $\lambda \rightarrow 0$  ML).

Such a method is the detection of polarized fluorescence light emitted from He atoms which are excited by EC during grazing scattering from a surface.<sup>13,38–40,42–45</sup> Under defined conditions, EC hysteresis loops are obtained by monitoring the Stokes parameter  $S/I$  as a function of the external magnetic field. The reversible part of the surface magnetization is related to the normalized parameter  $\Delta S/I = S/I(\uparrow) - S/I(\downarrow)$  with the Stokes parameter  $S/I(\uparrow)$  and  $S/I(\downarrow)$  for reversed settings of the magnetization. The results of the EC measurements are shown in the lower panel of Fig. 12. For 6 ML Co on 10 ML  $\text{Ni}_x\text{Mn}_{100-x}$  bilayers,  $\Delta S/I$  amounts to about 25–30 % for a low content of Ni  $0 \leq x \leq 5$  (region I) and for Ni-rich films with  $60 \leq x \leq 100$  (region III) for  $T=133$  and 300 K. This is equal to the value for a 6 ML Co single film because the magnetization of the whole film and the topmost surface layer is reversed during the field sweep. Similar behavior was found for the bilayer system 6 ML Co/15 ML  $\text{Fe}_x\text{Mn}_{100-x}$  containing an Fe-rich alloy with  $60 \leq x_{\text{Fe}} \leq 100$  or an Fe-poor layer with an Fe content of  $0 \leq x_{\text{Fe}} \leq 20$  at room temperature.<sup>13</sup>

For a Ni content of  $5 \leq x \leq 10$ ,  $\Delta S/I$  decreases to a value of about 5% and 2% for  $T=300$  K and 133 K, respectively. The reduction in  $\Delta S/I$  is due to an incomplete magnetization reversal. One part of the topmost surface layer is changed by the external magnetic field while another part is pinned as a result of the Co/NiMn coupling. The fraction of reversed surface magnetization is smallest for the intermediate concentration regime (region II) with a Ni content of  $10 \leq x \leq 30$  for  $T=300$  K and  $10 \leq x \leq 40$  for  $T=133$  K, respectively. For a Ni content of  $10 \leq x \leq 35$ , the determined values of the normalized Stokes parameter for  $T=133$  K with  $\Delta S/I \leq 3\%$  were plotted as gray full diamonds in the lower panel of Fig. 12, since it was not possible to record complete MOKE hysteresis loops with the maximum accessible field of  $H = \pm 200$  Oe in this Ni concentration range (region II). For higher Ni concentrations,  $\Delta S/I$  increases again for a Ni content from  $x=30$  up to 45 at room temperature and from  $x=40$  up to 55 at  $T=133$  K, respectively. This behavior of the magnetization reversal of the topmost surface layer is in accord with the results of the MOKE measurements on the entire film magnetization of Co/NiMn bilayer films on Cu(001). Thus, we observe no difference in surface and bulk magnetization, different from the bilayer system Co/ $\text{Fe}_x\text{Mn}_{100-x}$  on Cu(001) in the intermediate concentration regime ( $20 \leq x \leq 60$ ) due to a weakened exchange interaction at the surface and defects in the film structure.<sup>13</sup> However,

the different changes in  $\Delta \hat{I}_{\text{MOKE}}$  and  $\Delta S/I$  with increasing Ni content with  $10 \leq x \leq 40$  (region II) at  $T=300$  K are still not understand.

#### IV. SUMMARY

We have studied growth and magnetic properties of Co/ $\text{Ni}_x\text{Mn}_{100-x}$  bilayers in the ultrathin film limit with a total thickness below 25 ML. For a Ni content  $35 \leq x \leq 85$ , we observed pronounced layer-by-layer growth on the Cu(001) substrate at room temperature, which allows one to tune the interface morphology of Co/NiMn bilayers. In accordance with the study in Ref. 30 smooth single-crystalline equiatomic NiMn films with a high structural perfection, identified by a  $c(2 \times 2)$  LEED pattern, can be prepared on Cu(001).

For the magnetic characterization, we performed MOKE and EC measurements. Changes in the hysteresis loop, in particular, the enhancement of the coercivity  $H_C$  and the reduction in the normalized MOKE signal  $\Delta \hat{I}_{\text{MOKE}}$  and  $\Delta S/I$  in the EC measurements, are explained by the magnetic interface coupling due to the antiferromagnetic ordering in the  $\text{Ni}_x\text{Mn}_{100-x}$  alloys. From the large increase in the coercivity  $H_C$  for decreasing temperature, the  $\theta_{\text{Co}}^{-1}$  dependence of  $H_C$  from the Co thickness  $\theta_{\text{Co}}$ , and the vanishing exchange bias, we conclude a small AFM anisotropy for the investigated Co/NiMn bilayer system. In analogy to the system Co/ $\text{Fe}_x\text{Mn}_{100-x}$ /Cu(001),<sup>13</sup> the concentration dependence of the magnetic properties provides a classification into three regimes. The strongest interface coupling effects are found in the intermediate concentration regime with a Ni content  $10 \leq x \leq 40$  at a temperature of  $T=300$  K and  $5 \leq x \leq 50$  for  $T=133$  K above a critical NiMn thickness of about 8 ML. We conclude that the AFM order is established not only in equiatomic NiMn films with high structural perfection but, in particular, also for nonlayer-by-layer grown NiMn films. The strength of the AFM anisotropy in Co/NiMn bilayers depends on the chemical composition of the NiMn film rather than on the structural perfection of the bilayer films. Based on the comparison of MOKE and EC measurements, we found no difference in reversal behavior of the surface and bulk magnetization, which was observed for Co/FeMn bilayers in a recent study.<sup>13</sup>

#### ACKNOWLEDGMENTS

We thank the DFG (Project No. Wi 1336) for financial support, K. Maass and G. Lindenberg for their assistance in the preparation and running of the experiments. We are grateful to W. Kuch (FU Berlin) for helpful discussions.

\*Corresponding author; mbusch@physik.hu-berlin.de

<sup>1</sup>G. A. Prinz, *Phys. Today* **48**(4), 58 (1995).

<sup>2</sup>G. A. Prinz, *Science* **282**, 1660 (1998).

<sup>3</sup>W. H. Meiklejohn and C. P. Bean, *Phys. Rev.* **102**, 1413 (1956).

<sup>4</sup>W. H. Meiklejohn and C. P. Bean, *Phys. Rev.* **105**, 904 (1957).

<sup>5</sup>R. L. Stamps, *J. Phys. D* **33**, R247 (2000).

<sup>6</sup>J. Nogués and I. K. Schuller, *J. Magn. Magn. Mater.* **192**, 203 (1999).

- <sup>7</sup>A. E. Berkowitz and K. Takano, *J. Magn. Magn. Mater.* **200**, 552 (1999).
- <sup>8</sup>3d, 4d, and 5d Elements, Alloys and Compounds, Landolt Börnstein, New Series, Group III Vol. 19, Pt. A, edited by H. P. J. Wijn (Springer-Verlag, Berlin, 1986).
- <sup>9</sup>W. Kuch, F. Offi, L. I. Chelaru, M. Kotsugi, K. Fukumoto, and J. Kirschner, *Phys. Rev. B* **65**, 140408(R) (2002).
- <sup>10</sup>F. Offi, W. Kuch, and J. Kirschner, *Phys. Rev. B* **66**, 064419 (2002).
- <sup>11</sup>F. Offi, W. Kuch, L. I. Chelaru, K. Fukumoto, M. Kotsugi, and J. Kirschner, *Phys. Rev. B* **67**, 094419 (2003).
- <sup>12</sup>R. Thamankar, S. Bhagwat, and F. O. Schumann, *Phys. Rev. B* **69**, 054411 (2004).
- <sup>13</sup>J. Seifert, T. Bernhard, M. Gruyters, and H. Winter, *Phys. Rev. B* **76**, 224405 (2007).
- <sup>14</sup>S. S. P. Parkin, K. P. Roche, M. G. Samant, P. M. Rice, R. B. Beyers, R. E. Scheuerlein, E. J. O'Sullivan, S. L. Brown, J. Bucchigano, D. W. Abraham, Y. Lu, M. Rooks, P. L. Trouiloud, R. A. Wanner, and W. J. Gallagher, *J. Appl. Phys.* **85**, 5828 (1999).
- <sup>15</sup>E. Krén, E. Nagy, I. Nagy, L. Pál, and P. Szabó, *J. Phys. Chem. Solids* **29**, 101 (1968).
- <sup>16</sup>L. Pál, E. Krén, G. Kádár, P. Szabó, and T. Tarnóczy, *J. Appl. Phys.* **39**, 538 (1968).
- <sup>17</sup>J. S. Kasper and J. S. Kouvel, *J. Phys. Chem. Solids* **11**, 231 (1959).
- <sup>18</sup>D. Spisák and J. Hafner, *J. Phys.: Condens. Matter* **11**, 6359 (1999).
- <sup>19</sup>V. V. Godlevsky and K. M. Rabe, *Phys. Rev. B* **63**, 134407 (2001).
- <sup>20</sup>A. Sakuma, *J. Magn. Magn. Mater.* **187**, 105 (1998).
- <sup>21</sup>M. Wuttig, T. Flores, and C. C. Knight, *Phys. Rev. B* **48**, 12082 (1993).
- <sup>22</sup>M. Wuttig and C. C. Knight, *Phys. Rev. B* **48**, 12130 (1993).
- <sup>23</sup>W. L. O'Brien and B. P. Tonner, *J. Appl. Phys.* **76**, 6468 (1994).
- <sup>24</sup>W. L. O'Brien and B. P. Tonner, *Phys. Rev. B* **51**, 617 (1995).
- <sup>25</sup>T. Schulthess and W. Butler, *J. Appl. Phys.* **83**, 7225 (1998).
- <sup>26</sup>K. Nakamura, A. J. Freeman, D. Wang, L. Zhong, and J. Fernandez-de-Castro, *Phys. Rev. B* **65**, 012402 (2001).
- <sup>27</sup>S. Groudeva-Zotova, D. Elefant, R. Kaltofen, D. Tietjen, J. Thomas, V. Hoffmann, and C. M. Schneider, *J. Magn. Magn. Mater.* **263**, 57 (2003).
- <sup>28</sup>R. Thamankar, S. Bhagwat, and F. O. Schumann, *J. Phys.: Condens. Matter* **16**, 6029 (2004).
- <sup>29</sup>B. R. Malonda-Boungou, B. M'Passi-Mabiala, S. Meza-Aguilar, and C. Demangeat, *Surf. Sci.* **600**, 1763 (2006).
- <sup>30</sup>C. Tieg, W. Kuch, S. G. Wang, and J. Kirschner, *Phys. Rev. B* **74**, 094420 (2006).
- <sup>31</sup>C. L. Gao, A. Ernst, A. Winkelmann, J. Henk, W. Wulfhekkel, P. Bruno, and J. Kirschner, *Phys. Rev. Lett.* **100**, 237203 (2008).
- <sup>32</sup>T. Bernhard, M. Baron, M. Gruyters, and H. Winter, *Phys. Rev. Lett.* **95**, 087601 (2005).
- <sup>33</sup>R. Pfandzelter, T. Bernhard, and H. Winter, *Phys. Rev. Lett.* **90**, 036102 (2003).
- <sup>34</sup>H. Winter, K. Maass, S. Lederer, H. P. Winter, and F. Aumayr, *Phys. Rev. B* **69**, 054110 (2004).
- <sup>35</sup>F. Aumayr, G. Lakits, and H. P. Winter, *Appl. Surf. Sci.* **47**, 139 (1991).
- <sup>36</sup>M. Baron, T. Bernhard, M. Gruyters, and H. Winter, *Surf. Sci.* **600**, 3924 (2006).
- <sup>37</sup>T. Bernhard, J. Seifert, and H. Winter, *J. Phys.: Condens. Matter* **21**, 134001 (2009).
- <sup>38</sup>H. Winter, H. Hagedorn, R. Zimny, H. Nienhaus, and J. Kirschner, *Phys. Rev. Lett.* **62**, 296 (1989).
- <sup>39</sup>H. Winter, *Z. Phys. D: At., Mol. Clusters* **23**, 41 (1992).
- <sup>40</sup>J. Leuker, H. W. Ortjohann, R. Zimny, and H. Winter, *Surf. Sci.* **388**, 262 (1997).
- <sup>41</sup>R. Guenther, *Modern Optics* (Wiley, New York, 1990).
- <sup>42</sup>R. Pfandzelter and M. Potthoff, *Phys. Rev. B* **64**, 140405(R) (2001).
- <sup>43</sup>M. Gruyters, T. Bernhard, and H. Winter, *Phys. Rev. Lett.* **94**, 227205 (2005).
- <sup>44</sup>M. Busch, M. Gruyters, and H. Winter, *Surf. Sci.* **600**, 4166 (2006).
- <sup>45</sup>M. Busch, M. Gruyters, and H. Winter, *Surf. Sci.* **600**, 4598 (2006).
- <sup>46</sup>C. Liu, E. R. Moog, and S. D. Bader, *Phys. Rev. Lett.* **60**, 2422 (1988).
- <sup>47</sup>E. Mentz, A. Bauer, T. Günther, and G. Kaindl, *Phys. Rev. B* **60**, 7379 (1999).
- <sup>48</sup>M. H. Langelaar and D. O. Boerma, *Surf. Sci.* **436**, 237 (1999).
- <sup>49</sup>T. Flores, M. Hansen, and M. Wuttig, *Surf. Sci.* **279**, 251 (1992).
- <sup>50</sup>J. Shen, J. Giergiel, and J. Kirschner, *Phys. Rev. B* **52**, 8454 (1995).
- <sup>51</sup>P. Pouloupoulos, J. Lindner, M. Farle, and K. Baberschke, *Surf. Sci.* **437**, 277 (1999).
- <sup>52</sup>L. E. Davis, N. C. MacDonald, P. W. Palmberg, G. E. Riach, and R. E. Weber, *Handbook of Auger Electron Spectroscopy* (Perkin-Elmer, Eden Prairie, 1978).
- <sup>53</sup>M. P. Seah and W. A. Dench, *Surf. Interface Anal.* **1**, 2 (1979).
- <sup>54</sup>S. Tanuma, C. J. Powell, and D. R. Penn, *Surf. Interface Anal.* **17**, 911 (1991).
- <sup>55</sup>C. M. Schneider, P. Bressler, P. Schuster, J. Kirschner, J. J. de Miguel, R. Miranda, and S. Ferrer, *Vacuum* **41**, 503 (1990).
- <sup>56</sup>P. Krams, F. Lauks, R. L. Stamps, B. Hillebrands, and G. Güntherodt, *Phys. Rev. Lett.* **69**, 3674 (1992).
- <sup>57</sup>W. Weber, R. Allenspach, and A. Bischof, *Appl. Phys. Lett.* **70**, 520 (1997).
- <sup>58</sup>X. Gao, M. Salvietti, W. Kuch, C. M. Schneider, and J. Kirschner, *J. Electron Spectrosc. Relat. Phenom.* **113**, 137 (2001).
- <sup>59</sup>M. D. Stiles and R. D. McMichael, *Phys. Rev. B* **63**, 064405 (2001).
- <sup>60</sup>C. Mocuta, A. Barbier, S. Lafaye, P. Bayle-Guillemaud, and M. Panabière, *Phys. Rev. B* **68**, 014416 (2003).
- <sup>61</sup>L. Ding, P. F. Ladwig, X. Yan, and Y. A. Chang, *Appl. Phys. Lett.* **80**, 1186 (2002).
- <sup>62</sup>L. Péter, Z. Rolik, L. F. Kiss, J. Tóth, V. Weihnacht, C. M. Schneider, and I. Bakonyi, *Phys. Rev. B* **73**, 174410 (2006).
- <sup>63</sup>H. B. Zhao, D. Talbayev, G. Lüpke, A. T. Hanbicki, C. H. Li, M. J. van't Erve, G. Kioseoglou, and B. T. Jonker, *Phys. Rev. Lett.* **95**, 137202 (2005).
- <sup>64</sup>M. Kiwi, *J. Magn. Magn. Mater.* **234**, 584 (2001).